Original Research

Gentiopicroside alleviates acute myocardial infarction injury in rats by disrupting Nrf2/NLRP3 signaling

Fei Li[1*], Hongxiang Zhu[2*], Zijuan Chang[2] and Ying Li[2]

[1]The First Ward of Cardiovascular Medicine, Yantaishan Hospital, Yantai 264000, China; [2]Department of Emergency, Yantai Yuhuangding Hospital, Yantai 264000, China
*These authors contributed equally to this paper.
Corresponding authors: Zijuan Chang. Email: czj20192020@163.com; Ying Li. Email: ypklz@163.com

Impact statement

Acute myocardial infarction (AMI) is a form of myocardial ischemic necrosis that results from a reduction or cessation of blood supply to the coronary arteries. Gentiopicroside (GPS), a natural iridoid glycoside, has demonstrated pharmacological properties in animal models, including cholagogic, anti-hepatotoxic, anti-inflammatory, and anti-oxidant activities. Our investigation indicates that GPS may mitigate inflammatory responses and oxidative stress by modulating the Nrf2/NLRP3 signaling pathway in the context of AMI injury.

Abstract

The objective of the present investigation was to assess the protective impact of gentiopicroside (GPS) on acute myocardial infarction (AMI) through the modulation of NF-E2-related factor 2 (Nrf2)/nucleotide-binding oligomerization domain, leucine-rich repeat, and pyrin domain-containing 3 (NLRP3) signaling. H9c2 cells were subjected to varying concentrations of GPS, and subsequently, the cells and Sprague–Dawley (SD) rats were segregated into control, model, GPS, t-BHQ (an Nrf2 activator), and GPS + ML385 (an Nrf2 inhibitor) groups. The levels of superoxide dismutase (SOD) and malondialdehyde (MDA) were analyzed. Reactive oxygen species (ROS) and cell apoptosis were assessed, while Nrf2 and the expression of the NLRP3 inflammatory body signal pathway were evaluated using western blot and immunofluorescence techniques. The infarct area and pathological changes were also examined. Treatment with varying doses of GPS resulted in increased viability of H9c2 cells. Notably, the model group exhibited significantly elevated levels of cell apoptosis, MDA, and ROS compared to the control group, while SOD and Nrf2 levels were significantly reduced. Furthermore, the expression of NLRP3, cleaved caspase-1, interleukin (IL)-1β, and IL-18 were found to be augmented. Following the implementation of GPS in cells and animals, there was a notable reduction in MDA and ROS levels, a decrease in the rate of cellular apoptosis, and a mitigation of inflammation scores. In addition, there was an increase in the expression of SOD and Nrf2. However, the protective effects of GPS were negated when co-administered with ML385. GPS exhibits therapeutic properties in AMI rats by activating Nrf2 expression, thereby reducing the NLRP3 inflammatory body and alleviating the inflammatory response and oxidative stress of myocardial cells. GPS may hold promise as a potential drug for the treatment of AMI.

Keywords: Cell apoptosis, inflammation score, infarction area, oxidative stress, t-BHQ, ML385

***Experimental Biology and Medicine* 2023; 248: 1254–1266. DOI: 10.1177/15353702231199076**

Introduction

Cardiovascular diseases exhibit a significant burden of morbidity, disability, and mortality. Despite the employment of advanced and optimal treatment modalities, the global annual mortality rate due to cardiovascular and cerebrovascular diseases remains alarmingly high, with a staggering 15 million deaths, ranking it as the leading cause of death.[1]

The principal pathological mechanism underlying myocardial infarction, heart failure, and myocardial ischemia/reperfusion injury is widely acknowledged to be the apoptosis or necrosis of myocardial cells. The production of a significant quantity of reactive oxygen species (ROS) by myocardial cells is associated with long-term chronic hypoxia or acute ischemia/reperfusion.[2] Acute myocardial infarction (AMI) is a form of myocardial ischemic necrosis that results from a reduction or cessation of blood supply in the coronary artery.[3] The pathophysiological process of myocardial injury following AMI involves inflammation, immune response, apoptosis, autophagy, and mitochondrial dysfunction.[4] Oxidative stress and inflammatory response are crucial factors in the development of AMI.[5,6] An observation of decreased myocardial anti-oxidant capacity and heightened oxidative stress has been made during AMI.[7] Wei *et al.* indicated that the amelioration of AMI damage in rats can be achieved through the reduction of oxidative stress.[8]

Gentiopicroside (GPS), a natural iridoid glycoside, has been isolated from Gentiana manshurica Kitagawa, a commonly used herb in China. Its pharmacological effects, including anti-inflammatory, anti-hepatotoxic, and anti-oxidant activities, have been demonstrated in animal experiments.[9–11] Recent research has revealed that GPS regulates Nuclear factor kappa-B (NF-κB) signaling pathway to prevent kidney inflammation in diabetes mice.[12] Furthermore, GPS intensified trimetazidine-mediated inhibition of oxidative injury and inflammation in myocardial ischemia-reperfusion injury rats.[13] Based on these findings, it is reasonable to speculate that GPS may have a protective role in AMI.

The NLRP3 inflammasome is comprised of NOD-like receptor 3 containing CARD domain (NLRP3), apoptosis-related speck-like protein containing CARD domain (ASC), and pro-caspase-1.[14] It can induce the mature release of IL-1, IL-18, IL-33, and other pro-inflammatory factors by activating caspase-1, thus causing inflammation.[15] Recent studies have demonstrated that Nrf2 can exert a negative regulatory effect on NLRP3 inflammasome activity by inhibiting ROS-induced NLRP3 inflammasome activation.[16,17]

In this study, we investigated the effect of GPS on AMI *in vitro* and *in vivo*, particularly concentrating on the regulation of Nrf2 and NLRP3.

Materials and methods

Cell culture and grouping

H9C2 cells purchased from Procell (Wuhan, China). H9C2 added into DMEM (Invitrogen, USA) with 10% fetal bovine serum (FBS, Invitrogen, USA), cultured at 37°C with 5% CO_2. The process of oxygen glucose deprivation and reperfusion (OGD/R) model as follows, H9C2 cells were exposed to Earle's balanced salt solution with 0% O_2 for eight hours, followed by 12 h in DMEM with 95% air and 5% CO_2. Cells were first pretreated with different dose of GPS (12.5, 25, and 50 μM) for 24 h. In the next section, cells were grouped for five groups as follows: control, model, GPS (50 μM, Sigma-Aldrich, USA), t-BHQ (50 μM, Sigma-Aldrich, USA), GPS + ML385 (5 μM, Sigma-Aldrich, USA) groups.

CCK8 assay

H9C2 cells treatment as above description. CCK8 assay was carried out with a CCK8 kit (Solarbio, Beijing, China). In a word, 4×10^3 cells in 100 μL medium were seeded in 96-well plates. After the cells incubated for 48 h, then 10 μL CCK8 solution was added and cultured for another two hours. Microplate reader (Thermo Fisher Scientific, Inc., USA) was used to detect absorbance at 450 nm.

Transwell migration assay

In brief, 1×10^5 H9C2 cells were seeded into 24-well Transwell inserts (Corning Costar Corporation, USA) and cultured in the complete media. A 4% formaldehyde solution was used to fix migrated cells on the bottom surface, and 0.5% crystal violet (Beyotime, Shanghai, China) was used to stain them. The number of migrated cells was counted by an optical microscope (Olympus, Japan).

Detection of oxidative stress mediators

Superoxide dismutase (SOD) and malondialdehyde (MDA) levels were all obtained from corresponding kits (Nanjing Jiancheng Bioengineering Institute, Nanjing, China) in accordance with the manufacturer's protocols.

Dichlorodihydrofluorescein diacetate assay

H9C2 cells were incubated with dichlorodihydrofluorescein diacetate assay (DCFH-DA; 10 μmol/L, Beyotime, Shanghai, China) for 10 min at 37°C after different treatment. After three washes in DMEM, flow cytometric (FACScan, BD Bioscience, USA) immediately detected the cells. The process was performed referring to a previous study.[18]

Annexin-V/PI apoptosis detection assay

Annexin-V-FITC/PI apoptosis detection kit (Beyotime, Shanghai, China) was used to investigate H9C2 cells apoptosis rate. In a word, H9C2 cells were incubated in six-well plates and cultured after different treatment for 48 h. Then collecting the cells, they were rinsed with phosphate-buffered saline (PBS) and resuspended in 600 μL Annexin-V-binding buffer. H9C2 cells apoptotic rate was evaluated by flow cytometry.

Animals and induction of models

A total of 60 Sprague–Dawley (SD) rats (8–10 weeks, 270 ± 10 g) were acquired from the Jinan Peng Yue Experimental Animal Breeding Co. Ltd, Certificate No.: SCXK (Lu) - 20180030). Rats were divided into sham (control, no ligation was performed), AMI (model, with an equal volume of dissolvant), AMI + GPS (GPS, 50 mg/kg/d, intragastric administration), AMI + t-BHQ (t-BHQ, a Nrf2 activator, 50 mg/kg/d, intragastric administration), and AMI + GPS + ML385 (GPS + ML385, ML385 is a Nrf2 inhibitor, 30 mg/kg/d, intraperitoneal injected)[19] groups. Drugs were administrated for seven consecutive days preoperatively. In the AMI model, rats were anesthetized intraperitoneally with 1% pentobarbitalsodium (60 mg/kg, R&D system, USA) and mechanically ventilate after endotracheal intubation with an animal ventilator. We induced AMI by left anterior descending (LAD) coronary artery ligation. Electrocardiograms (ECGs) demonstrating pathological Q waves and/or ST elevations confirmed AMI. Left ventricular end-diastolic dimension (LVEDD) and left ventricular end-systolic dimension (LVESD) were measured. Left ventricular ejection fraction (LVEF) and left ventricular fractional shortening (LVFS) were used to evaluate the systolic function of the hearts. LVEF was calculated as $((LVEDD)3 - (LVESD)3]/(LVEDD)3] \times 100\%$ and LVFS was calculated as $[(LVEDD - LVESD)/LVEDD) \times 100\%$. All animal procedures were granted by the Ethics Committee of Animal Experiments of the Yantai Yuhuangding Hospital and followed the Guide for Care and Use of Laboratory Animals. The flow chart could be found in the supplementary materials.

Tetrazolium chloride (TTC) staining

Myocardial tissue was taken and rapidly frozen at –20°C for 20 min in order to facilitate slicing. Slices were placed in TTC at 37°C for 20 min away from light, with a concentration of 2%.

Following fixation with 4% paraformaldehyde for 24 h, slices were photographed and analized by Image J software.[20]

Haematoxylin–eosin staining of the heart tissues

Myocardial tissues were immersed in 4% paraformaldehyde and embedded in paraffin to prepare 5-μm slices. After the slices were deparaffinized and rehydrated, haematoxylin–eosin (H&E) was used to stain the slices. Images were obtained under a microscope (Olympus, Tokyo, Japan). The inflammatory scores of myocardial tissues were calculated according to a published study.[21] As part of scoring criteria inflammatory cell were scored on 0: no inflammation; 1: <5% inflammation; 2: 5–10% inflammation; 3: 10–25% inflammation; 4: >25% inflammation.

TUNEL

The apoptotic cells in heart sections were marked after incubation with TUNEL reaction mixture solution, then DAPI staining was used to determine the total number of myocardial cells. The sections were observed under a laser confocal microscope (Leica, Germany) and photographed.

Dihydroethidium assay

The heart sections were stained with 20 nmol/L dihydroethidium (DHE, Sigma) at 37°C for 15 min. At excitation/emission wavelengths of 488/610 nm under a laser confocal microscope (Leika, Germany), the sections were observed and photographed.

Immunofluorescence

A 6.0-μm thick myocardial tissue sample was fixed with 4% paraformaldehyde and permeabilized with 0.2% Triton X-100. It was then blocked for one hour with 5% bovine serum albumin (BSA, R&D system, USA). Then the slices were incubated with NLRP3 antibody at 4°C overnight. Finally, the slices were incubated with the corresponding fluorescent dye-conjugated secondary antibody at room temperature for one hour, nuclei counterstained with DAPI (Abcam, UK) according to the instructions.

Western blot

After different treatments, radioimmunoprecipitation assay lysis buffer (RIPA, Beyotime) was used to extract total proteins in cells and tissues at 4°C for 30 min. Using electrophoresis, proteins were separated and transferred to a Polyvinylidene Fluoride (PVDF) membrane. This study used the following primary antibodies: anti-Nrf2 (1:1000, Abcam), anti-HO-1 (1:1000, Abcam), anti-NLRP3 (1:1000, Abcam), anti-ASC (1:1000, Abcam), anti-cleaved caspase-1 (1:1000, Cell Signaling Technology), anti-cleaved-IL-1β (1:1000, Cell Signaling Technology), anti-IL-1β (1:500, Cell Signaling Technology), anti-IL-18 (1:1000, Abcam), anti-Bcl-2 (1:1000, Abcam), and anti-Bax (1:1000, Abcam). As a next step, Tris buffered saline with tween®20 (TBST) was used to wash the PVDF membrane three times with five minutes for each, followed by the second antibody goat anti-rabbit (1:3000, Abcam) was added. A proprietary chemiluminescence kit (Beyotime) was used to visualize the specific protein bands, then the bands quantified by the Image J software (NIH, USA). Initially, target proteins were corrected over inactive glyceraldehyde 3-phosphate dehydrogenase (GAPDH) expression and then as fold changes from controls.

Statistical analysis

GraphPad Prism 8.0 (Manufacturer, USA) was used to perform statistical analysis. Results were expressed as mean ± standard deviation (SD). One-way analysis of variance and Dunnett's test were used to compare multiple groups. $P < 0.05$ was considered statistically significant.

Results

GPS protects H9C2 cells against OGD/R-induced injury

We first investigated the effects of GPS on OGD/R induced injury. H9C2 cells were treated with different dosage of GPS before OGD/R model. We found that GPS treatment ameliorated the cells viability compared to OGD/R group (Figure 1(a), $P < 0.05$). In the following experiments, we divided cells into five groups with different treatments. As presented in Figure 1(b), the result of CCK8 assay indicated that GPS and t-BHQ treatment increased the cell viability, when cells treated with GPS + ML385, the increasing effect of GPS was weakened, indicated that ML385 treatment could decreased the enhancement effect of GPS. In order to confirm the effect of GPS on cells, we further used transwell assay. The results presented that H9C2 cells migration was significantly decreased after OGD/R (Figure 1(c) and (d), $P < 0.05$). GPS treatment markedly improved the migration ability compared to model group ($P < 0.05$), t-BHQ also partly improved the migration ability ($P < 0.05$). However, the enhancement of GPS was reversed by ML385 treatment.

GPS attenuates H9C2 cells injury by reducing oxidative stress

We further investigated the oxidative stress of H9C2 cells after OGD/R and different treatment. The results obtained from the preliminary analysis of SOD, MDA, and ROS were presented in Figure 2. It is apparent from this figure that the level of SOD in model group significantly decreased compared to the control group (Figure 2(a), $P < 0.05$), whereas the levels of MDA and ROS were increased in the model group (Figure 2(b) and (c), $P < 0.05$). However, GPS and t-BHQ treatment markedly reversed the increasing of MDA and ROS. Unfortunately, the use of ML385 reversed the promotion effect of GPS ($P < 0.05$).

GPS protects H9C2 cells against cells apoptosis

We then assessed the effect of GPS on H9C2 cells against cells apoptosis. A comparison of the control and model groups revealed the increasing apoptosis cells in the model group (Figure 3, $P < 0.05$). Compared with the model group, GPS treatment decreased H9C2 cells apoptosis, whereas ML385 treatment obviously reversed GPS-induced cells apoptosis reduction.

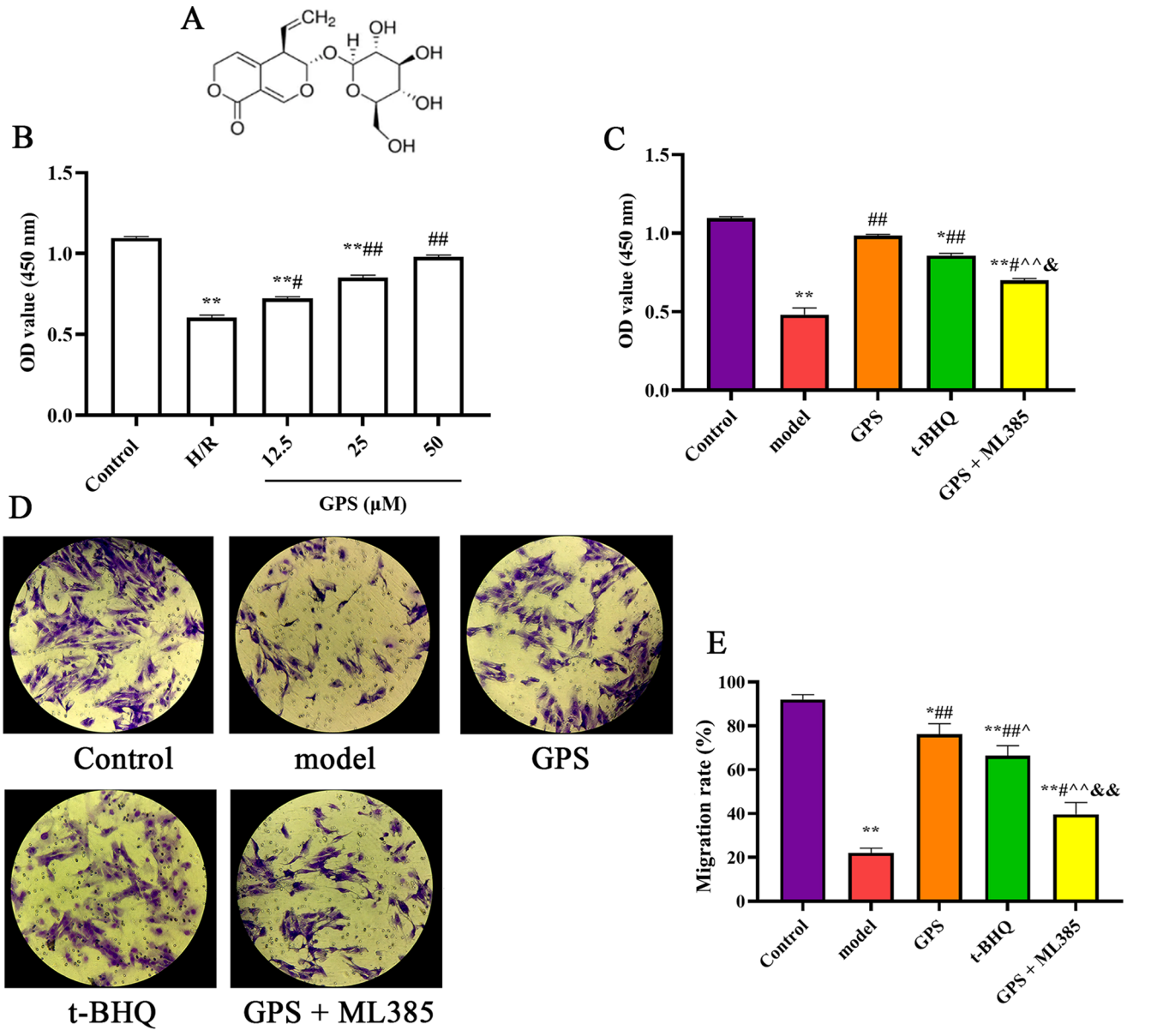

Figure 1. GPS promotes H9C2 cells proliferation ability: (a) chemical structure of GPS, (b) GPS improved the viability of H9C2 cells after H/R, (c) viability of H9C2 cells treated with different drugs according to grouping, GPS promoted the viability of H9C2 cells, (d) transwell assay was used to investigate the migration ability of H9C2 cells (Scale bar: 100 μm), (e) bar graph depicting the rate of H9C2 cell migration, GPS could promote the migration of H9C2 cells. $n=5$. $^{*}P<0.05$, $^{**}P<0.01$, compared to control group; $^{\#}P<0.05$, $^{\#\#}P<0.01$, compared to model group; $^{\wedge}P<0.05$, $^{\wedge\wedge}P<0.01$, compared to GPS group; $^{\&}P<0.05$, $^{\&\&}P<0.01$, compared to t-BHQ group.

The protective effect of GPS on H9C2 cells injury was related to Nrf2/NLRP3 signaling

The results obtained from western blot were shown in Figure 4. The expression level of Nrf2 in H9C2 cells significantly decreased after OGD/R, while the NLRP3, cleaved caspase-1, IL-1β, and IL-18 levels were obviously increased ($P<0.05$). As expect, GPS, t-BHQ treatment augmented the expression of Nrf2, while reduced NLRP3, cleaved caspase-1, IL-1β, and IL-18. However, the effect of GPS was reversed when co-treated with ML385.

GPS ameliorates AMI

As shown in Table 1, LVEF and LVFS were significantly decreased in model group than those in the control group. GPS and t-BHQ treatment improved the decreasing of LVEF and LVFS. After AMI, the myocardial infarct size was increased. GPS treatment effectively alleviated the myocardial infarct size (Figure 5(a) and (b), $P<0.05$). In the control group, no pathological changes were found in myocardial cells. Myocardial fibers of rats in model group were broken, cells were swollen, and a large number of inflammatory cells were observed (Figure 5(c)). GPS treatment decreased the inflammation score of heart tissue (Figure 5(d)). Compared to t-BHQ group, the GPS treatment was more effective. However, the effect was decreased when co-treated with ML385.

GPS attenuates myocardial tissue injury by reducing oxidative stress

The next section of the study was concerned with the oxidative stress. The results of the SOD, MDA, and ROS are

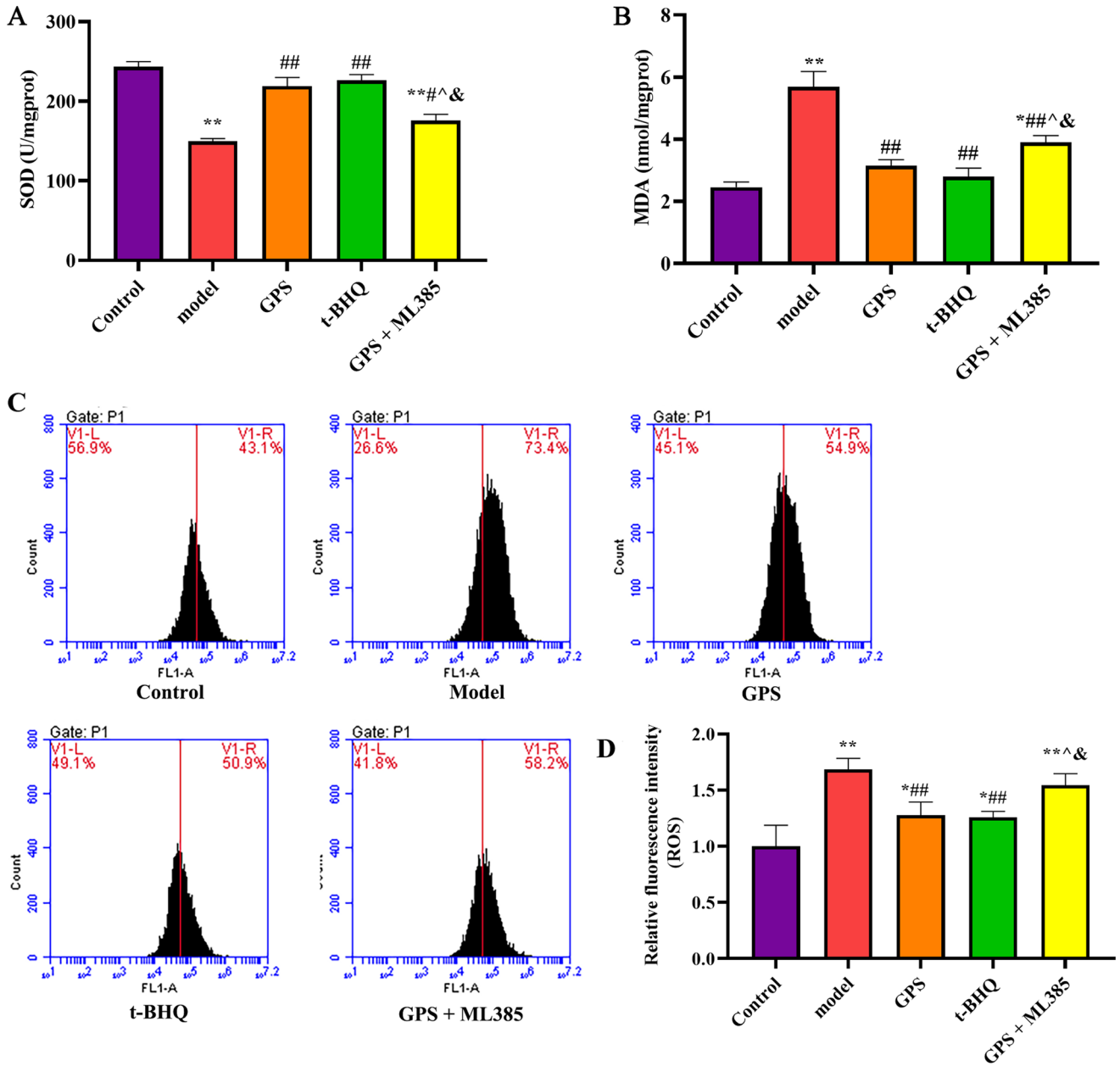

Figure 2. GPS alleviated oxidative stress in H9C2 cells: (a) the level of SOD was assessed by corresponding SOD kit, SOD content increased after GPS or t-BHQ treatment, (b) the level of MDA was assessed by corresponding MDA kit, MDA content decreased after GPS or t-BHQ treatment, (c) ROS was detected by flow cytometry using DCFA-DA kit, (d) the column diagram shows the quantification of ROS by relative fluorescent density, the relative fluorescent density was decreased after GPS or t-BHQ treatment. $n = 5$. $^{**}P < 0.01$, compared to control group; $^{\#}P < 0.05$, $^{\#\#}P < 0.01$, compared to model group; $^{\wedge}P < 0.05$, compared to GPS group; $^{\&}P < 0.05$, compared to t-BHQ group.

displayed in Figure 6. The level of SOD in model group significantly decreased compared to the control group ($P < 0.05$), whereas the levels of MDA and ROS were increased. GPS and t-BHQ treatment significantly reversed the increasing of MDA and ROS. Unfortunately, the administration of ML385 was reversed the protective effect of GPS ($P < 0.05$).

GPS protects myocardial tissue against cells apoptosis

The findings presented in Figure 7 demonstrate that GPS treatment effectively reduces myocardial cell apoptosis in comparison to the model group ($P < 0.05$). In addition, T-BHQ treatment also reduces myocardial cell apoptosis, albeit to a lesser extent than GPS. Notably, a significant difference persists between the GPS and t-BHQ groups. However, ML385 treatment obviously reversed GPS-induced cells apoptosis reduction. We also detected the expression levels of Bcl-2 and Bax. After AMI, the expression levels of Bcl-2 decreased while Bax increased. The observed pattern of alteration was in accordance with the outcomes obtained through the TUNEL assay.

The protective effect of GPS was related to Nrf2/NLRP3 signaling

Consistent with the results in H9C2 cells, the expression levels of Nrf2 and HO-1 in myocardial tissue significantly

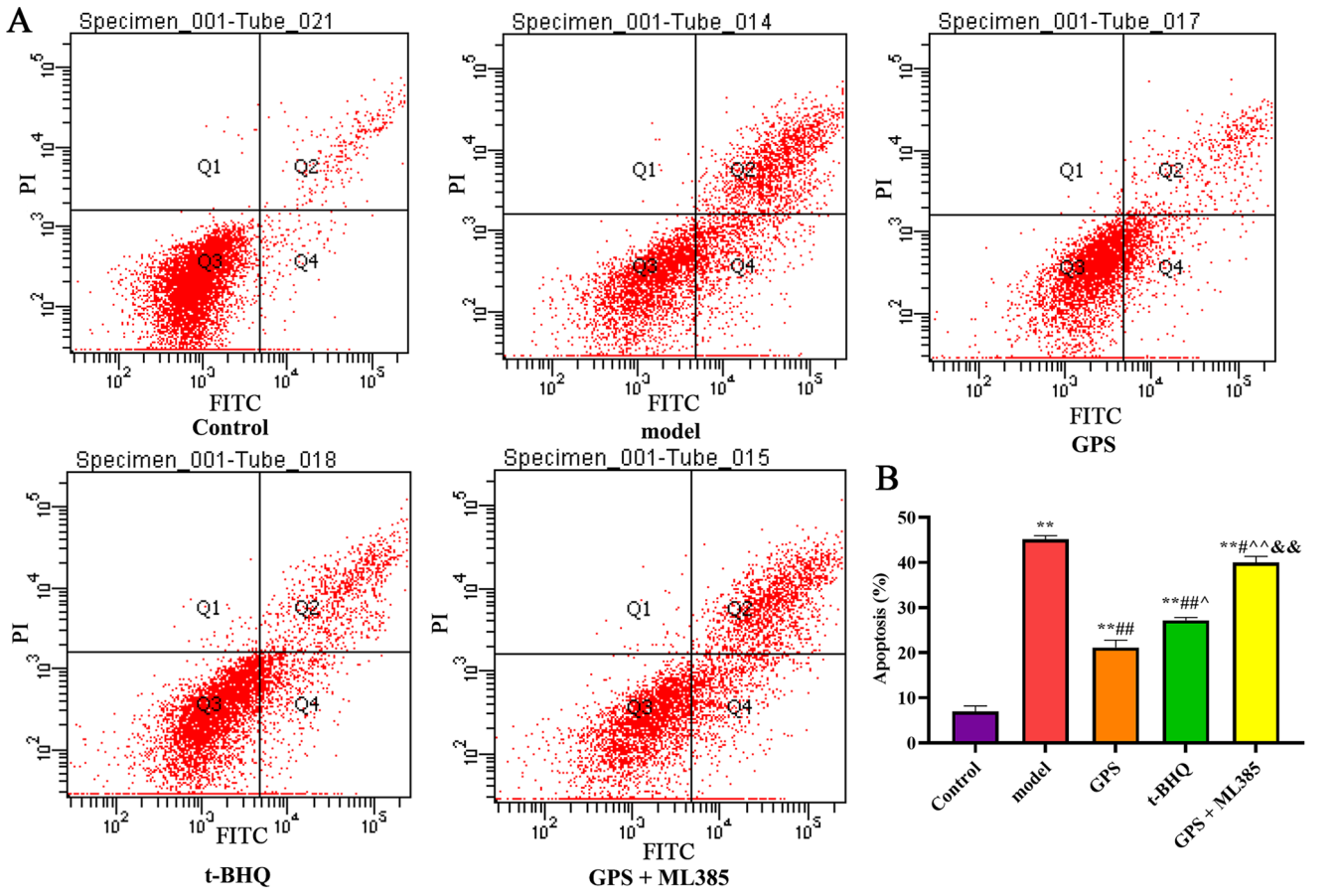

Figure 3. GPS ameliorated H9C2 cells apoptosis: (a) H9C2 cell was assessed by flow cytometry, (b) the column diagram shows the apoptotic rates of all groups, GPS treatment decreased the apoptotic rates of H9C2 cells. $n = 5$. $^{**}P < 0.01$, compared to control group; $^{\#}P < 0.05$, $^{\#\#}P < 0.01$, compared to model group; $^{\wedge\wedge}P < 0.01$, compared to GPS group; $^{\&\&}P < 0.01$, compared to t-BHQ group.

decreased after AMI, while the NLRP3, ASC, cleaved caspase-1, cleaved IL-1β, IL-1β, and IL-18 levels obviously augmented ($P < 0.05$). As expect, GPS, t-BHQ treatment augmented the expression of Nrf2 and HO-1, while reduced NLRP3, ASC, cleaved caspase-1, cleaved IL-1β, IL-1β, and IL-18. However, the effect of GPS was significantly reversed when co-treated with ML385 (Figure 8, $P < 0.05$).

Discussion

According to clinical research, myocardial infarction is the primary cause of cardiovascular disease and mortality. Restoring blood supply to the heart is considered the most effective treatment for myocardial infarction.[22] However, reperfusion may exacerbate myocardial injury by inducing excessive production of oxygen-free radicals and apoptosis in myocardial cells. These mechanisms are part of a complex signal network that contributes to AMI injury. GPS, a traditional Chinese medicine, is commonly used to treat pain and inflammatory diseases. Prior research has suggested that GPS may impact the gastric mucosal injury in mice through anti-inflammatory and anti-oxidant mechanisms.[23] Nevertheless, the impact of GPS on AMI remains largely indeterminate in academic literature. T-BHQ is a widely used anti-oxidant, also known as Nrf2 activator. ML385 is a potent Nrf2 inhibitor. In this study, we administered varying doses of GPS to H9C2 cells prior to OGD/R injury and observed that GPS enhanced cell viability following OGD/R. To elucidate the underlying mechanism of this effect, we employed t-BHQ as a comparative agent. Our findings demonstrate that GPS significantly promotes cell migration.

Excessive production of ROS is a significant contributor to oxidative stress, which plays a crucial role in the pathogenesis of myocardial ischemia-reperfusion injury.[24] The degree of cellular oxidative damage can be reflected by the content of MDA, the ultimate product of lipid peroxidation. SOD is an important anti-oxidant enzyme that inhibits free radical production and maintains metabolic balance. However, the overproduction of ROS can deplete SOD, disrupt the oxidation-antioxidation balance, and trigger oxidative stress damage and cell apoptosis. The present investigation demonstrates that pretreatment with GPS can effectively augment the SOD level in H9C2 cells, diminish the ROS level, and impede MDA production subsequent to OGD/R. These findings suggest that GPS may mitigate H9C2 cell damage induced by OGD/R by enhancing the anti-oxidant capacity of H9C2 cells. In addition, GPS confers protection against H9C2 cell apoptosis.

The decline in endogenous anti-oxidant defense, due to the reduction of transcription factor Nrf2, triggers the activation of NLRP3 inflammatory bodies, particularly during the aging process.[25] Upon activation of NLRP3 inflammatory

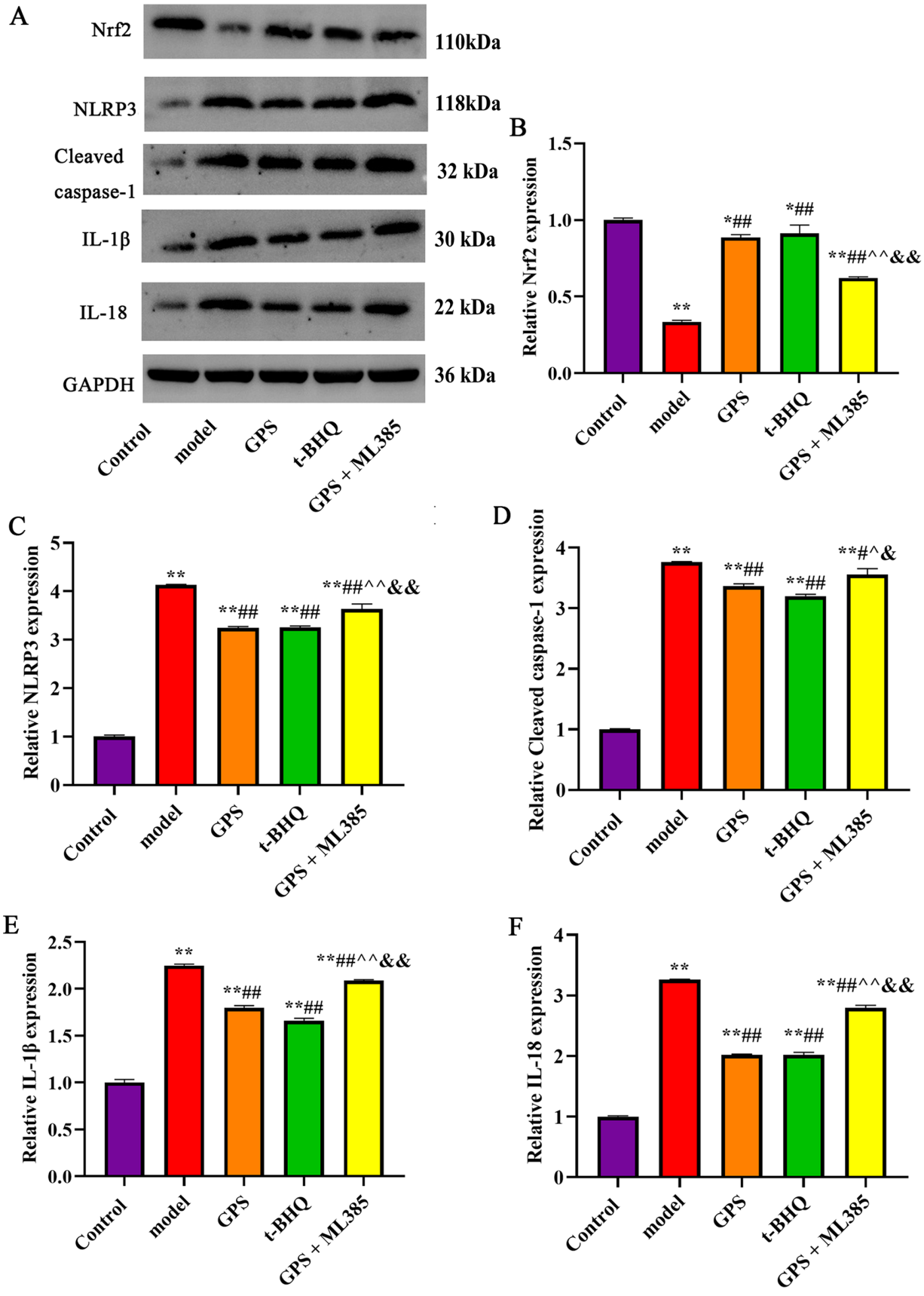

Figure 4. GPS attenuates H9C2 cells injury by inhibiting NLRP3 via upregulating Nrf2: (a) Western blot was used to detect the expression of proteins; the column diagram shows the quantification of Nrf2 (b), NLRP3 (c), cleaved caspase-1 (d), IL-1β (e), and IL-18 (f), GPS treatment enhanced the expression level of Nrf2, while reduced NLRP3, cleaved caspase-1, IL-1β, and IL-18 expression. $n=3$. $^{*}P<0.05$, $^{**}P<0.01$, compared to control group; $^{\#}P<0.05$, $^{\#\#}P<0.01$, compared to model group; $^{\wedge}P<0.05$, $^{\wedge\wedge}P<0.01$, compared to GPS group; $^{\&}P<0.05$, $^{\&\&}P<0.01$, compared to t-BHQ group.

Table 1. Comparison of cardiac function of rats in different group ($n=5$, mean ± SD).

Groups	LVEDD (mm)	LVESD (mm)	LVEF (%)	LVFS (%)
Control	5.62 ± 0.25	3.79 ± 0.09	68.93 ± 5.45	32.46 ± 3.95
model	7.36 ± 0.21**	6.07 ± 0.07**	43.68 ± 5.01**	17.47 ± 2.39**
GPS	6.24 ± 0.18**##	4.34 ± 0.08**##	66.21 ± 3.68##	30.42 ± 2.57##
t-BHQ	6.39 ± 0.16**##	4.49 ± 0.04**##	64.98 ± 3.49##	29.57 ± 2.29##
GPS + ML385	6.85 ± 0.10**##	4.79 ± 0.11**##	65.78 ± 3.45##	30.11 ± 2.28##

LVEDD: left ventricular end-diastolic dimension; LVESD: left ventricular end-systolic dimension; LVEF: left ventricular ejection fraction; LVFS: left ventricular fractional shortening; GPS: gentiopicroside; t-BHQ: tert-butylhydroquinone.
**$P<0.01$, compared to control group; ##$P<0.01$, compared to model group.

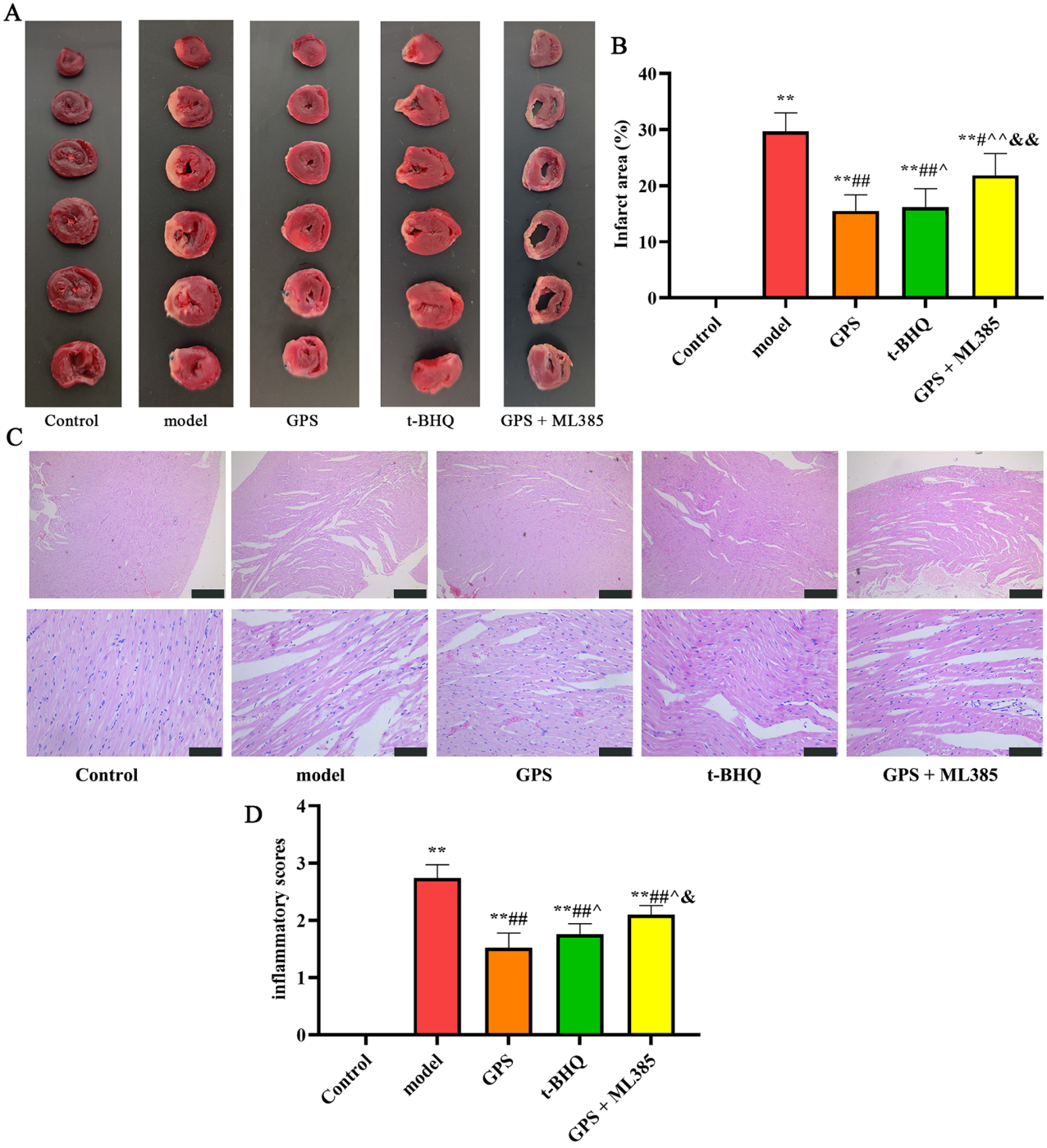

Figure 5. Effect of GPS on AMI in rats: (a) TTC staining was used to assess the myocardial infarction, (b) infarct area was presented as white area/total area, GPS treatment improved the infarct area of rat heart tissue, (c) pathological changes in myocardial tissues were presented by H&E staining (Scale bar: 500 μm, 100 μm), (d) inflammatory index of myocardial tissues were qualified by inflammation score, GPS treatment reduced inflammation score of myocardial tissues. $n=5$. **$P<0.01$, compared to control group; #$P<0.05$, ##$P<0.01$, compared to model group; ^$P<0.05$, ^^$P<0.01$, compared to GPS group; &$P<0.05$, &&$P<0.01$, compared to t-BHQ group.

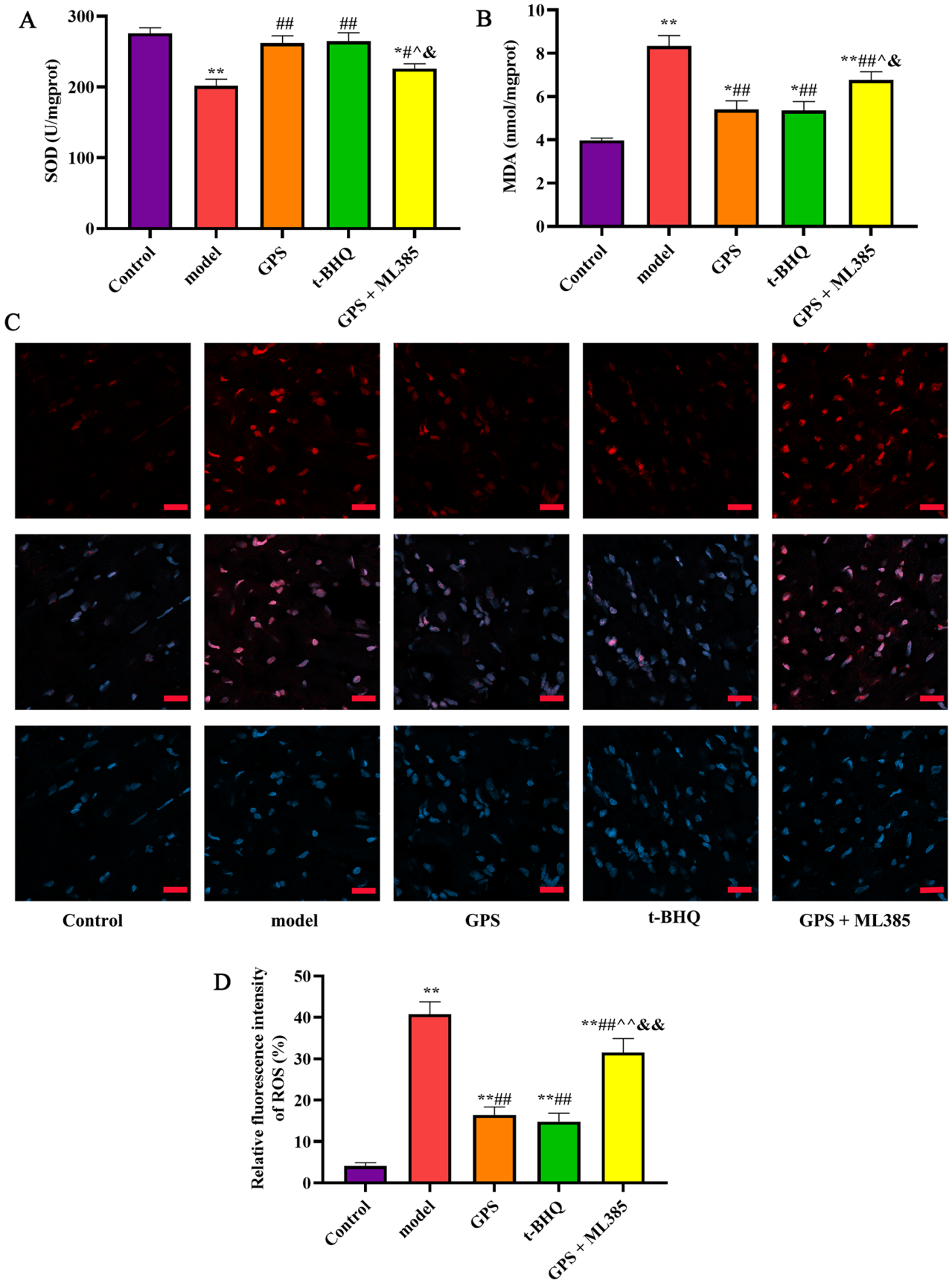

Figure 6. GPS alleviated oxidative stress in myocardial cells: (a) The level of SOD was assessed by corresponding SOD kit, SOD content increased after GPS or t-BHQ treatment, (b) the level of MDA was assessed by corresponding MDA kit, MDA content decreased after GPS or t-BHQ treatment, (c) the level of ROS was detected DHE kit (Scale bar: 20 μm), (d) the column diagram shows the quantification of ROS, GPS, or t-BHQ treatment reduced the ROS level in myocardial tissues. $n=5$. $^{*}P<0.05$, $^{**}P<0.01$, compared to control group; $^{\#}P<0.05$, $^{\#\#}P<0.01$, compared to model group; $^{\wedge}P<0.05$, $^{\wedge\wedge}P<0.01$, compared to GPS group; $^{\&}P<0.05$, $^{\&\&}P<0.01$, compared to t-BHQ group.

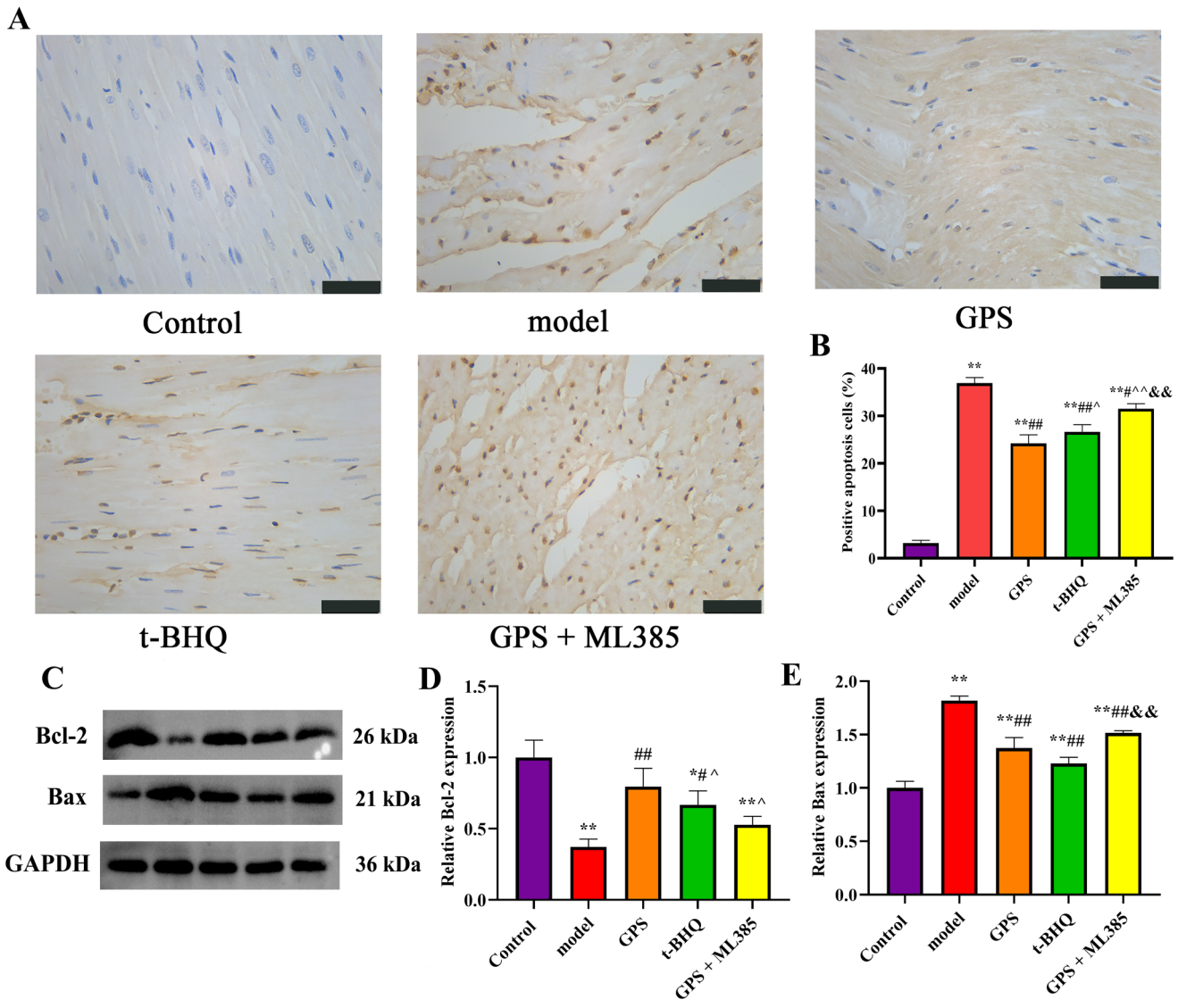

Figure 7. GPS ameliorated myocardial cells apoptosis: (a) TUNEL was used to assess the cells apoptosis in myocardial tissue (Scale bar: 50 μm), (b) the column diagram shows the apoptotic rates of all groups. GPS treatment reduced cell apoptosis; $n=5$, (c) Western blot was used to detect the expression levels Bcl-2 and Bax; the column diagram shows the quantization of Bcl-2 (d) and Bax (e) expression levels; GPS treatment reduced the Bcl-2 expression, while enhanced Bax expression; $n=3$. $^{**}P<0.01$, compared to control group; $^{\#}P<0.05$, $^{\#\#}P<0.01$, compared to model group; $^{\wedge}P<0.05$, $^{\wedge\wedge}P<0.01$, compared to GPS group; $^{\&\&}P<0.01$, compared to t-BHQ group.

bodies, pro-cassase-1 undergoes processing and activation into active caspase-1, leading to the cleavage and release of IL-1β and IL-18 precursors, which contribute to the pathogenesis of various inflammatory diseases.[26] Previous studies have demonstrated that Nrf2 can mitigate neuroinflammation by inhibiting NLRP3.[27,28] In light of the anti-inflammatory and anti-oxidant properties of GPS, we investigated the expression of Nrf2 and NLRP3 to gain novel insights into GPS treatment. Our western blot analysis revealed that GPS treatment significantly enhanced the expression of Nrf2 and reduced that of NLRP3, as anticipated. However, the levels of NLRP3, cleaved caspase-1, IL-1β, and IL-18 were reduced in H9C2 cells following OGD/R after GPS treatment.

The subsequent section of the investigation focused on an *in vivo* experiment to confirm the protective impact of GPS in AMI rats as assessed by oxidative stress and apoptosis. The findings revealed that GPS treatment effectively mitigated pathological alterations and myocardial infarction area. Furthermore, GPS treatment significantly elevated SOD, decreased ROS levels, and suppressed MDA production after AMI, indicating that GPS reduced myocardial tissue damage. This suggests that GPS may mitigate myocardial tissue damage resulting from AMI by enhancing the anti-oxidant capacity of myocardial cells. In addition, GPS treatment was observed to decrease the rate of cell apoptosis in myocardial tissue. We also investigated the expression levels of Bcl-2 and Bax. We found that GPS and t-BHQ treatment improved the expression level of Bcl-2 while decreased Bax expression. Mechanistically, we evaluated the expression levels proteins relate to Nrf2/NLPR3 signaling and found that GPS treatment augmented the expression of Nrf2, HO-1 while reducing NLRP3, ASC, cleaved caspase-1, cleaved IL-1β, IL-1β, and IL-18 expression. These findings are consistent with prior research.[27,28] Notably, the protective effects of GPS were partially reversed by ML385. However, given the intricate regulatory mechanisms involved in AMI, further investigation is required to determine whether GPS can exert its protective effects through alternative pathways.

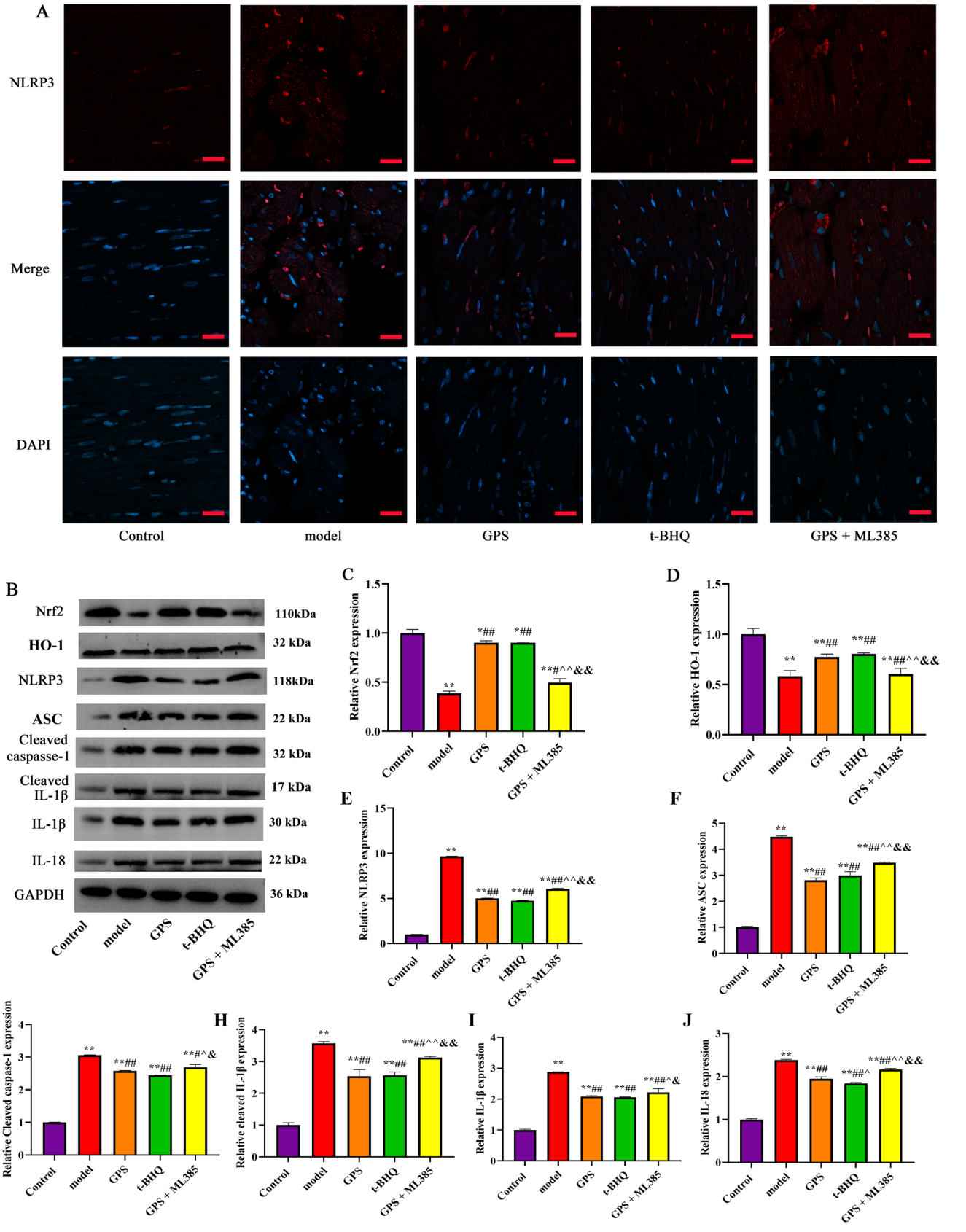

Figure 8. GPS attenuates myocardial tissue injury via Nrf2/NLRP3 signaling: (a) immunofluorescence assay was used to investigate the expression of NLPR3 in myocardial tissue (Scale bar: 20 μm), GPS treatment reduced the expression of NLPR3, (b) Western blot was used to detect the expression of proteins; the column diagram shows the quantification of Nrf2 (c), HO-1 (d), NLRP3 (e), ASC (f), cleaved caspase-1 (g), cleaved-IL-1β (h), IL-1β (i), and IL-18 (j) expression levels. GPS treatment enhanced the expression levels of Nrf2 and HO-1 levels, while reduced NLRP3, ASC, cleaved caspase-1, cleaved-IL-1β, IL-1β, and IL-18 expression. $n = 3$. $^{*}P < 0.05$, $^{**}P < 0.01$, compared to control group; $^{\#}P < 0.05$, $^{\#\#}P < 0.01$, compared to model group; $^{\wedge}P < 0.05$, $^{\wedge\wedge}P < 0.01$, compared to GPS group; $^{\&}P < 0.05$, $^{\&\&}P < 0.01$, compared to t-BHQ group.

Conclusions

In summary, the utilization of GPS exhibits the capacity to mitigate the inflammatory response and oxidative stress of myocardial cells subsequent to AMI injury, while concurrently serving a protective function by decreasing the occurrence of apoptosis in myocardial cells. Our investigation indicates that the underlying mechanism of GPS's efficacy is associated with the Nrf2/NLRP3 signaling pathway.

AUTHORS' CONTRIBUTIONS

FL and ZC participated in the study design. FL, HZ, ZC, and YL carried out the experimental work, data collection, data interpretation, and preparation of the article. All authors read and approved the final article.

DECLARATION OF CONFLICTING INTERESTS

The author(s) declared no potential conflicts of interest with respect to the research, authorship, and/or publication of this article.

FUNDING

The author(s) received no financial support for the research, authorship, and/or publication of this article.

ORCID ID

Zijuan Chang https://orcid.org/0000-0002-2850-2147

SUPPLEMENTAL MATERIAL

Supplemental material for this article is available online.

REFERENCES

1. Roth GA, Johnson C, Abajobir A, Abd-Allah F, Abera SF, Abyu G, Ahmed M, Aksut B, Alam T, Alam K, Alla F, Alvis-Guzman N, Amrock S, Ansari H, Ärnlöv J, Asayesh H, Atey TM, Avila-Burgos L, Awasthi A, Banerjee A, Barac A, Bärnighausen T, Barregard L, Bedi N, Belay Ketema E, Bennett D, Berhe G, Bhutta Z, Bitew S, Carapetis J, Carrero JJ, Malta DC, Castañeda-Orjuela CA, Castillo-Rivas J, Catalá-López F, Choi JY, Christensen H, Cirillo M, Cooper L, Jr., Criqui M, Cundiff D, Damasceno A, Dandona L, Dandona R, Davletov K, Dharmaratne S, Dorairaj P, Dubey M, Ehrenkranz R, El Sayed Zaki M, Faraon EJA, Esteghamati A, Farid T, Farvid M, Feigin V, Ding EL, Fowkes G, Gebrehiwot T, Gillum R, Gold A, Gona P, Gupta R, Habtewold TD, Hafezi-Nejad N, Hailu T, Hailu GB, Hankey G, Hassen HY, Abate KH, Havmoeller R, Hay SI, Horino M, Hotez PJ, Jacobsen K, James S, Javanbakht M, Jeemon P, John D, Jonas J, Kalkonde Y, Karimkhani C, Kasaeian A, Khader Y, Khan A, Khang YH, Khera S, Khoja AT, Khubchandani J, Kim D, Kolte D, Kosen S, Krohn KJ, Kumar GA, Kwan GF, Lal DK, Larsson A, Linn S, Lopez A, Lotufo PA, El Razek HMA, Malekzadeh R, Mazidi M, Meier T, Meles KG, Mensah G, Meretoja A, Mezgebe H, Miller T, Mirrakhimov E, Mohammed S, Moran AE, Musa KI, Narula J, Neal B, Ngalesoni F, Nguyen G, Obermeyer CM, Owolabi M, Patton G, Pedro J, Qato D, Qorbani M, Rahimi K, Rai RK, Rawaf S, Ribeiro A, Safiri S, Salomon JA, Santos I, Santric Milicevic M, Sartorius B, Schutte A, Sepanlou S, Shaikh MA, Shin MJ, Shishehbor M, Shore H, Silva DAS, Sobngwi E, Stranges S, Swaminathan S, Tabarés-Seisdedos R, Tadele Atnafu N, Tesfay F, Thakur JS, Thrift A, Topor-Madry R, Truelsen T, Tyrovolas S, Ukwaja KN, Uthman O, Vasankari T, Vlassov V, Vollset SE, Wakayo T, Watkins D, Weintraub R, Werdecker A, Westerman R, Wiysonge CS, Wolfe C, Workicho A, Xu G, Yano Y, Yip P, Yonemoto N, Younis M, Yu C, Vos T, Naghavi M, Murray C. Global, regional, and national burden of cardiovascular diseases for 10 causes, 1990 to 2015. *J Am Coll Cardiol* 2017;**70**:1–25
2. Zhu H, Jin Q, Li Y, Ma Q, Wang J, Li D, Zhou H, Chen Y. Melatonin protected cardiac microvascular endothelial cells against oxidative stress injury via suppression of IP3R-[Ca^{2+}]c/VDAC-[Ca^{2+}]m axis by activation of MAPK/ERK signaling pathway. *Cell Stress Chaperones* 2018;**23**:101–13
3. Ye J, Xiao R, Wang X, He R, Liu Z, Gao J. Effects and mechanism of renal denervation on ventricular arrhythmia after acute myocardial infarction in rats. *BMC Cardiovasc Disord* 2022;**22**:544
4. Fu Z, Jiao Y, Wang J, Zhang Y, Shen M, Reiter RJ, Xi Q, Chen Y. Cardioprotective role of melatonin in acute myocardial infarction. *Front Physiol* 2020;**11**:366
5. Ong SB, Hernández-Reséndiz S, Crespo-Avilan GE, Mukhametshina RT, Kwek XY, Cabrera-Fuentes HA, Hausenloy DJ. Inflammation following acute myocardial infarction: multiple players, dynamic roles, and novel therapeutic opportunities. *Pharmacol Ther* 2018;**186**:73–87
6. Piamsiri C, Maneechote C, Siri-Angkul N, Chattipakorn SC, Chattipakorn N. Targeting necroptosis as therapeutic potential in chronic myocardial infarction. *J Biomed Sci* 2021;**28**:25
7. Hassan MQ, Akhtar MS, Akhtar M, Ali J, Haque SE, Najmi AK. Edaravone protects rats against oxidative stress and apoptosis in experimentally induced myocardial infarction: biochemical and ultrastructural evidence. *Redox Rep* 2015;**20**:275–81
8. Wei YJ, Wang JF, Cheng F, Xu HJ, Chen JJ, Xiong J, Wang J. miR-124-3p targeted SIRT1 to regulate cell apoptosis, inflammatory response, and oxidative stress in acute myocardial infarction in rats via modulation of the FGF21/CREB/PGC1α pathway. *J Physiol Biochem* 2021;**77**:577–87
9. Ren G, Zhang Q, Xia P, Wang J, Fang P, Jin X, Peng X, Xu Y, Zhang J, Zhao L. Synthesis and biological evaluation of gentiopicroside derivatives as novel cyclooxygenase-2 inhibitors with anti-inflammatory activity. *Drug Des Devel Ther* 2023;**17**:919–35
10. Li X, Zhang Y, Jin Q, Xia KL, Jiang M, Cui BW, Wu YL, Song SZ, Lian LH, Nan JX. Liver kinase B1/AMP-activated protein kinase-mediated regulation by gentiopicroside ameliorates P2X7 receptor-dependent alcoholic hepatosteatosis. *Br J Pharmacol* 2018;**175**:1451–70
11. He M, Hu C, Chen M, Gao Q, Li L, Tian W. Effects of Gentiopicroside on activation of NLRP3 inflammasome in acute gouty arthritis mice induced by MSU. *J Nat Med* 2022;**76**:178–87
12. Xiao H, Sun X, Liu R, Chen Z, Lin Z, Yang Y, Zhang M, Liu P, Quan S, Huang H. Gentiopicroside activates the bile acid receptor Gpbar1 (TGR5) to repress NF-kappaB pathway and ameliorate diabetic nephropathy. *Pharmacol Res* 2020;**151**:104559
13. Wang Y, Sheng Y, Ji N, Zhang H. Gentiopicroside enhances the protective effect of trimetazidine against myocardial ischemia-reperfusion injury via the AMPK/NLRP3 inflammasome signaling. *J Biochem Mol Toxicol* 2023;**7**:e23366
14. Broz P, Dixit VM. Inflammasomes: mechanism of assembly, regulation and signalling. *Nat Rev Immunol* 2016;**16**:407–20
15. Guo C, Fu R, Wang S, Huang Y, Li X, Zhou M, Zhao J, Yang N. NLRP3 inflammasome activation contributes to the pathogenesis of rheumatoid arthritis. *Clin Exp Immunol* 2018;**194**:231–43
16. Liu X, Zhang X, Ding Y, Zhou W, Tao L, Lu P, Wang Y, Hu R. Nuclear factor E2-related factor-2 negatively regulates NLRP3 inflammasome activity by inhibiting reactive oxygen species-induced NLRP3 priming. *Antioxid Redox Signal* 2017;**26**:28–43
17. Rzepecka J, Pineda MA, Al-Riyami L, Rodgers DT, Huggan JK, Lumb FE, Khalaf AI, Meakin PJ, Corbet M, Ashford ML, Suckling CJ, Harnett MM, Harnett W. Prophylactic and therapeutic treatment with a synthetic analogue of a parasitic worm product prevents experimental arthritis and inhibits IL-1β production via NRF2-mediated counter-regulation of the inflammasome. *J Autoimmun* 2015;**60**:59–73
18. Qi S, Guo L, Yan S, Lee RJ, Yu S, Chen S. Hypocrellin A-based photodynamic action induces apoptosis in A549 cells through ROS-mediated mitochondrial signaling pathway. *Acta Pharm Sin B* 2019;**9**:279–93
19. Liu D, Wang H, Zhang Y, Zhang Z. Protective effects of chlorogenic acid on cerebral ischemia/reperfusion injury rats by regulating oxidative stress-related Nrf2 pathway. *Drug Des Devel Ther* 2020;**14**:51–60

20. Van Hout GP, Bosch L, Ellenbroek GH, De Haan JJ, Van Solinge WW, Cooper MA, Arslan F, De Jager SC, Robertson AA, Pasterkamp G, Hoefer IE. The selective NLRP3-inflammasome inhibitor MCC950 reduces infarct size and preserves cardiac function in a pig model of myocardial infarction. *Eur Heart J* 2017;**38**:828–36
21. Wang C, Wang L, Wang L. Paeoniflorin improves autoimmune myocarditis in young rat by inhibiting CXCR5 to reduce follicular helper T cells. *Autoimmunity* 2022;**55**:632–9
22. Meyer K, Hodwin B, Ramanujam D, Engelhardt S, Sarikas A. Essential role for premature senescence of myofibroblasts in myocardial fibrosis. *J Am Coll Cardiol* 2016;**67**:2018–28
23. Yang Y, Wang Z, Zhang L, Yin B, Lv L, He J, Chen Z, Wen X, Qiao B, Sun W, Fang M, Zhang Y. Protective effect of gentiopicroside from Gentiana macrophylla Pall. in ethanol-induced gastric mucosal injury in mice. *Phytother Res* 2018;**32**:259–66
24. Kalogeris T, Baines CP, Krenz M, Korthuis RJ. Cell biology of ischemia/reperfusion injury. *Int Rev Cell Mol Biol* 2012;**298**: 229–317
25. Schmidlin CJ, Dodson MB, Madhavan L, Zhang DD. Redox regulation by NRF2 in aging and disease. *Free Radic Biol Med* 2019;**134**:702–7
26. Ising C, Venegas C, Zhang S, Scheiblich H, Schmidt SV, Vieira-Saecker A, Schwartz S, Albasset S, McManus RM, Tejera D, Griep A, Santarelli F, Brosseron F, Opitz S, Stunden J, Merten M, Kayed R, Golenbock DT, Blum D, Latz E, Buée L, Heneka MT. NLRP3 inflammasome activation drives tau pathology. *Nature* 2019;**575**:669–73
27. Xu LL, Wu YF, Yan F, Li CC, Dai Z, You QD, Jiang ZY, Di B. 5-(3,4-Difluorophenyl)-3-(6-methylpyridin-3-yl)-1,2,4-oxadiazole (DDO-7263), a novel Nrf2 activator targeting brain tissue, protects against MPTP-induced subacute Parkinson's disease in mice by inhibiting the NLRP3 inflammasome and protects PC12 cells against oxidative stress. *Free Radic Biol Med* 2019;**134**:288–303
28. Xin W, Wang Q, Zhang D, Wang C. A new mechanism of inhibition of IL-1β secretion by celastrol through the NLRP3 inflammasome pathway. *Eur J Pharmacol* 2017;**814**:240–7

(Received January 15, 2023, Accepted July 20, 2023)